atmosphere

Westerly Variations in the Eastern Tibetan Plateau since the Last Interglacial Revealed by the Grain-Size Records of the Ganzi Loess

Shengli Yang, Jiantao Zhou, Zixuan Chen, Pushuang Li, Chen Wen, Xuechao Xu and Qiong Li *

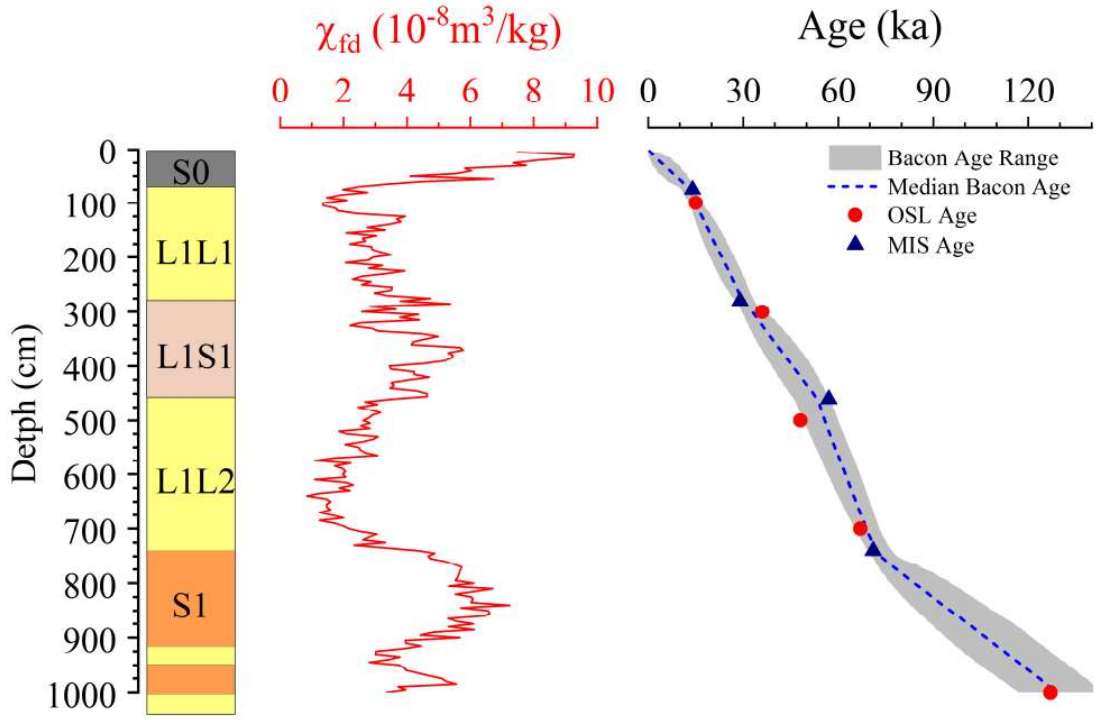

Figure S1. Lithology and Bacon age–depth model of the Xinshi (XS) section.

Table S1. Comparison of decomposition results in grain-size end-member analysis of loess sediments in different regions (unit of EM, μm).

Regions	EM1	Dynamic source	EM2	Dynamic source	EM3	Dynamic source	EM4	Dynamic source	EM5	Dynamic source	Literature source
Yellow River source area	1–3	process of weathering and pedogenesis	6–12	long-existing high-level Westerlies	20–40	Westerlies and TPM	36–70	Westerlies and TPM	177–257	strong valley wind	(Jia et al., 2022)
Shandong Province	1	weathering and pedogenesis	5.62	high altitude westerly winds	15.85	settling in the form of floating dust	35.48	winter monsoon	70.79	dust storms	(Kong et al., 2021)
Southern Tibetan Plateau	8.1	pedogenesis and the MLW	66.4	derived from nearby, sandy sources	127	EM3 and EM2 are controlled by the same dynamic mechanism	243	dust storms			(Gao et al., 2021)
Yili Basin	1	pedogenic component	5	Westerlies	13	near-ground suspension component	35	near-ground suspension component			(Wang et al., 2019)

NE Tibetan Plateau	0.3–1	pedogenic intensity	5–7	westerly winds	10–17	westerly winds	25–31	low-level winds	44–63	low-level winds	(Li et al., 2020)
Altun Shan	4.8	background dust	19.6	surface winds							(Xu et al., 2018)
Altun Shan	4.7	background dust	20.6	surface winds							(Xu et al., 2018)
The southern margin of the CLP	2.83	high airflow and product of the weathering or pedogenesis	8.56	westerly	20.96	EAWM					(Hou et al., 2021)
Ningxia	1–10	background deposition of dust	10–100	East Asian winter monsoon	>100	nearby					(Jiang et al., 2017)
Lop Nur, Tarim Basin	63	major dust outbreaks	30	low-level winds during major dust outbreaks	10	high-altitude westerly	4	runoff and the related volume of the Lop Nur paleolake			(Liu et al., 2019)
The northern slope of the Tianshan	5.3	Westerlies	10.5	Westerlies	39.8	surface winds					(Duan et al., 2020)
Tien Shan	1.6	pedogenesis	11	high altitude Westerlies	39.8	near-surface winds					(Jia et al., 2018)

References

1. Duan, F.; An, C.; Wang, W.; Herzschuh, U.; Zhang, M.; Zhang, H.; Liu, Y.; Zhao, Y.; Li, G. Dating of a late Quaternary loess section from the northern slope of the Tianshan Mountains (Xinjiang, China) and its paleoenvironmental significance. *Quat. Int.* **2020**, *544*, 104–112. https://doi.org/10.1016/j.quaint.2020.02.034.
2. Gao, F.; Yang, J.; Wang, S.; Wang, Y.; Li, K.; Wang, F.; Ling, Z.; Xia, D. Variation of the winter mid-latitude Westerlies in the Northern Hemisphere during the Holocene revealed by aeolian deposits in the southern Tibetan Plateau. *Quat. Res.* **2022**, *107*, 104–112.
3. Hou, K.; Qian, H.; Zhang, Y.T.; Zhang, Q.Y.; Qu, W.G. New insights into loess formation on the southern margin of the Chinese Loess Plateau. *Catena* **2021**, *204*, 105444.
4. Jia, J.; Liu, H.; Gao, F.; Xia, D. Variations in the westerlies in Central Asia since 16 ka recorded by a loess section from the Tien Shan Mountains. *Palaeogeogr. Palaeoclimatol. Palaeoecol.* **2018**, *504*, 156–161.
5. Jia, Y.-N.; Zhang, Y.; Huang, C.C.; Wang, N.; Qiu, H.; Wang, H.; Xiao, Q.; Chen, D.; Lin, X.; Zhu, Y.; et al. Late Pleistocene-Holocene aeolian loess-paleosol sections in the Yellow River source area on the northeast Tibetan Plateau: Chronostratigraphy, sediment provenance, and implications for paleoclimate reconstruction. *Catena* **2022**, *208*, 105777. https://doi.org/10.1016/j.catena.2021.105777.
6. Jiang, H.C.; Wan, S.M.; Ma, X.L.; Zhong, N.; Zhao, D.B. End-member modeling of the grain-size record of Sikouzi fine sediments in Ningxia (China) and implications for temperature control of Neogene evolution of East Asian winter monsoon: *PLoS* One **2017**, *12*, 10.
7. Kong, F.; Xu, S.; Han, M.; Chen, H.; Miao, X.; Kong, X.; Jia, G. Application of grain size endmember analysis in the study of dust accumulation processes: A case study of loess in Shandong Province, East China. *Sediment. Geol.* **2021**, *416*, 105868. https://doi.org/10.1016/j.sedgeo.2021.105868.
8. Li, X.; Peng, T.; Ma, Z.; Li, M.; Li, P.; Feng, Z.; Guo, B.; Yu, H.; Ye, X.; Zhang, J.; et al. The Sources and Transport Dynamics of Eolian Sediments in the NE Tibetan Plateau Since 6.7 Ma. *Geochem. Geophys. Geosystems* **2020**, *21*, e2019GC008682. https://doi.org/10.1029/2019gc008682.
9. Liu, J.; Wang, R.; Zhao, Y.; Yang, Y. A 40,000-year record of aridity and dust activity at Lop Nur, Tarim Basin, northwestern China. *Quat. Sci. Rev.* **2019**, *211*, 208–221. https://doi.org/10.1016/j.quascirev.2019.03.023.
10. Wang, L.; Jia, J.; Zhao, H.; Liu, H.; Duan, Y.; Xie, H.; Zhang, D.D.; Chen, F. Optical dating of Holocene paleosol development and climate changes in the Yili Basin, arid central Asia. *Holocene* **2019**, *29*, 1068–1077. https://doi.org/10.1177/0959683619831432.
11. Xu, Y.; Li, J.; Pan, F.; Yang, B.; Tang, Y.; Bi, Y.; Li, T.; Yue, L.; Wingate, M.T. Late Neogene aridification and wind patterns in the Asian interior: Insight from the grain-size of eolian deposits in Altun Shan, northern Tibetan Plateau. *Palaeogeogr. Palaeoclim. Palaeoecol.* **2018**, *511*, 532–540. https://doi.org/10.1016/j.palaeo.2018.09.017.